Supporting Information: Effect of O_2 on plasma-based dry reforming of methane: Revealing the optimal gas composition via experiments and modelling of an atmospheric pressure glow discharge

Stein Maerivoet*[1], Bart Wanten*[1], Robin De Meyer[1,2], Morgane Van Hove[1], Senne Van Alphen[1] and Annemie Bogaerts[1]

[1] Research group PLASMANT, Department of Chemistry, University of Antwerp, Universiteitsplein 1, BE-2610 Wilrijk-Antwerp, Belgium

[2] Research group EMAT, Department of Physics, University of Antwerp, Groenenborgerlaan 171, 2020 Antwerp, Belgium

E-mail: stein.maerivoet@uantwerpen.be; bart.wanten@uantwerpen.be; annemie.bogaerts@uantwerpen.be

* Shared first authors

Pages: 22
Figures: 3
Tables: 7

Contents

S.1. Experimental details

S.1.1. Agilent 990 Micro Gas Chromatograph

We used an Agilent 990 Micro GC for our gas analysis. Only two GC channels are used, each with a column and thermal conductivity detector (TCD): channel 1 and 2. Channel 1 uses a molsieve 5A column and Ar as carrier gas; permanent gases (CO, H_2, O_2, and CH_4), are separated and detected on this channel. Channel 2 uses a PoraPLOT U column and He as carrier gas; it separates CO_2, C_2H_2, C_2H_4 and C_2H_6 from each other and from the permanent gasses. Both these channels utilize a CP PoraBOND Q as pre-column.

Before entering a channel, the gas mixture is heated to 70 °C by an electrically heated cable to ensure elimination of any liquid fraction from the gas chromatograph. Gases with boiling points below 70 °C are caught in the cold trap, to ensure safety of the GC channels.

S.1.2. Calculation of performance metrics

Table S1 summarizes the metrics used in this work to describe the reaction performance, accompanied by the corresponding symbol, unit and formula. The measured concentrations obtained through the GC are expressed in % and noted in general as $c_{i/j}^{in/out}$, with i and j indicating whether it is describing a reactant or product, respectively, and in and out indicating whether it is an input or an output fraction. The factor α is a correction factor for the volumetric expansion during reaction, and will be further discussed in section S.1.3. In the energy cost formulas, the plasma power is noted as P_{plasma} and expressed in kW, the total input flow rate as φ_{in} and expressed in L s^{-1}. Finally, $\mu_{i/j}^{A}$ refers to the number of atoms A in one molecule of i or j.

Table S1: Overview of performance metrics used in this work, with corresponding symbol, unit and formula. Note that the energy cost is given here in kJ L^{-1}, but it can also be expressed in e.g. kJ mol^{-1} or eV $molecule^{-1}$.

Performance metric	Symbol	Unit	Formula
Conversion (absolute)	χ_i^{abs}	-	$\frac{c_i^{in} - \alpha \cdot c_i^{out}}{c_i^{in}}$
Conversion (total)	χ^{tot}	-	$\sum_i c_i^{in} \cdot \chi_i^{abs}$
Energy cost (conversion)	EC_χ	kJ L^{-1} converted reactant	$\frac{P_{plasma}}{\varphi_{in} \cdot \chi^{tot}}$
Energy cost (syngas)	EC_{syngas}	kJ L^{-1} syngas	$\frac{P_{plasma}}{\varphi_{in} \cdot \alpha \cdot \left(c_{CO}^{out} + c_{H_2}^{out} \right)}$
Syngas ratio	SR	NA	$\frac{c_{H_2}^{out}}{c_{CO}^{out}}$
Product selectivity	S_j^A	-	$\frac{\mu_j^A \cdot \alpha \cdot c_j^{out}}{\sum_i \left(\mu_i^A \cdot \left(c_i^{in} - \alpha \cdot c_i^{out} \right) \right)}$

S.1.3. Correction factors for gas expansion

The conversion of gases is often accompanied by a change in moles. The theoretical DRM reaction doubles its amount of substance (see DRM reaction in the Introduction of the main paper). As a consequence, the gas expands, leading to a lower concentration of each species. When only using the measured concentrations to calculate e.g. conversion, the latter will be overestimated, simply due to the rise in total volume/number of moles. Simultaneously, among the components produced during the reaction, some may end up as liquid in the cold trap. Loss of these condensed components influences the concentrations of the remaining gas components. As shown by Pinhão et al.[1], Cleiren et al.[2] and Wanten et al.[3], a correction factor α can be implemented to account for this change in total volume/number of moles.

The correction factor, α, is the ratio of the flow rate, φ, at the GC and the flow rate at the inlet (both measured with a bubble flow meter, see figure 2 in the main paper, during plasma and blank measurements, respectively):

$$\alpha = \frac{\varphi_{out}\ (L\ min^{-1})}{\varphi_{in}\ (L\ min^{-1})} \qquad [SI.1]$$

Afterwards, a second correction factor, α', is defined as the correction factor using the flow rate after the plasma. As mentioned before, the difference between the flow rate right after the plasma and the flow rate at the GC is the condensation of liquids (mostly water – see section S.1.4) in the cold trap. The flow rate created by water vapour and the effect on the correction factor, α, can be calculated using an estimated H_2O concentration based on the O atom balance. The correction factor, α', can thus be calculated using the estimated molar fraction in the gas mixture of water, c'_{H_2O}, before condensation took place:

$$\alpha' = \alpha\left(1 - c'_{H_2O}\right)^{-1} \qquad [SI.2]$$

S.1.4. Cold trap liquid fraction analysis and H_2O balance calculations

As explained in the main paper (section 2.2), a cold trap is used to condense all products with low boiling points to liquid form. The liquid fraction collected in the cold trap was analysed by a Thermo Focus SSL GC with Stabilwax column and FID. Table S2 shows the concentrations of the main components present (besides H_2O) for each condition. It is clear that the concentrations of the main components, i.e., CH_3OH and CH_3CH_2OH, are at maximum 0.04 % and 0.003 %, respectively. Hence, we can approximate the liquid sample as pure H_2O.

Unfortunately, this means that the APGD appears not suitable to create valuable oxygenated compounds. The model of Maerivoet et al.[4] supports this claim, because it predicts the immediate destruction of these compounds in the modelled plasma chemistry.

Table S2: Liquid analysis results of the cold trap liquid samples, for all conditions investigated

$CO_2/CH_4/O_2$ fraction (% / % / %)	CH_3OH (%)	CH_3CH_2OH (%)
65 / 35 / 0	0.00	0.000

63 / 34 / 3	0.01	0.000
61 / 33 / 6	0.02	0.000
59 / 32 / 9	0.01	0.000
57 / 31 / 12	0.02	0.002
55 / 30 / 15	0.01	0.000
49 / 36 / 15	0.02	0.002
42.5 / 42.5 / 15	0.03	0.003
36 / 49 / 15	0.04	0.002

As H_2O cannot be detected in our GC, its concentration formed in the plasma is calculated from the O-atom balance, defined as:

$$b_O = \frac{\alpha \cdot (\sum_i \mu_{i,O} \cdot c_i^{plasma} + \sum_j \mu_{j,O} \cdot c_j^{plasma}) + \alpha' \cdot \sum_k \mu_{k,O} \cdot c_k{}'}{\sum_i \mu_{i,O} \cdot c_i^{plasma}} = 1 \qquad \text{[SI.3]}$$

Here, μ depicts the number of O atoms in a molecule. The ratio of all O atoms in blank and plasma measurements has to be 1. The first term of the numerator depicts the sum of all molecules containing an O atom found in the GC, here CO_2, O_2 and CO. The second term describes the fraction of O atom-carrying molecules not found in the GC, here H_2O. The denominator describes the inlet molecules containing O, here CO_2 and O_2. Using correction factor α', we are able to estimate the H_2O concentration as:

$$\sum_k \mu_{k,O} \cdot c_k{}' \cong c'_{H_2O}$$

With $\mu_{k,O}$ being 1, since H_2O has one O-atom. The use of c' instead of c denotes the concentration at the end of the plasma, since no H_2O is measured in the GC. The combination of these formulas results in the concentration of H_2O formed in the plasma. This c'_{H_2O} and α' is also used instead of α and c_j^{out} in the selectivity formula from section S.1.2, to calculate the selectivity of H_2O.

S.1.5. Safety precautions

Working with high voltages, in a $CO_2/CH_4/O_2$ plasma producing CO, requires some safety precautions, as listed below:

- Figure S1 depicts the explosion limit of an $CO_2/CH_4/O_2$ gas mixture. We stayed below 15 % O_2 to ensure staying out of any explosion zone. The literature described several plasma reactors operating at higher O_2 fractions, but figure S1 shows this is dangerous and should be considered carefully.
- Pressure relief valves releasing at 5 bar were also present in the setup to eliminate eventual explosions due to built-up pressure.

- An insulation mat is present next to the high voltage fume hoods to ensure no current can flow through any person towards the ground. The voltages used in this work, in the range of 10 kV, can create sparks up to a few centimetres long, which might be further than expected.
- CO detectors were present at all times during plasma measurements, both on working personnel as well as stationary detectors on the walls.
- All reactors are placed in a fume hood and the power supply can only be activated once the glass window of the fume hood is lowered.
- At all times multiple people were present in the lab, to act in case of emergency.
- A grounding stick was used to ground all remaining charges of all used experimental equipment after each measurement. Charge can accumulate and linger on conductive equipment if it is not in contact with the built-in grounding pin.

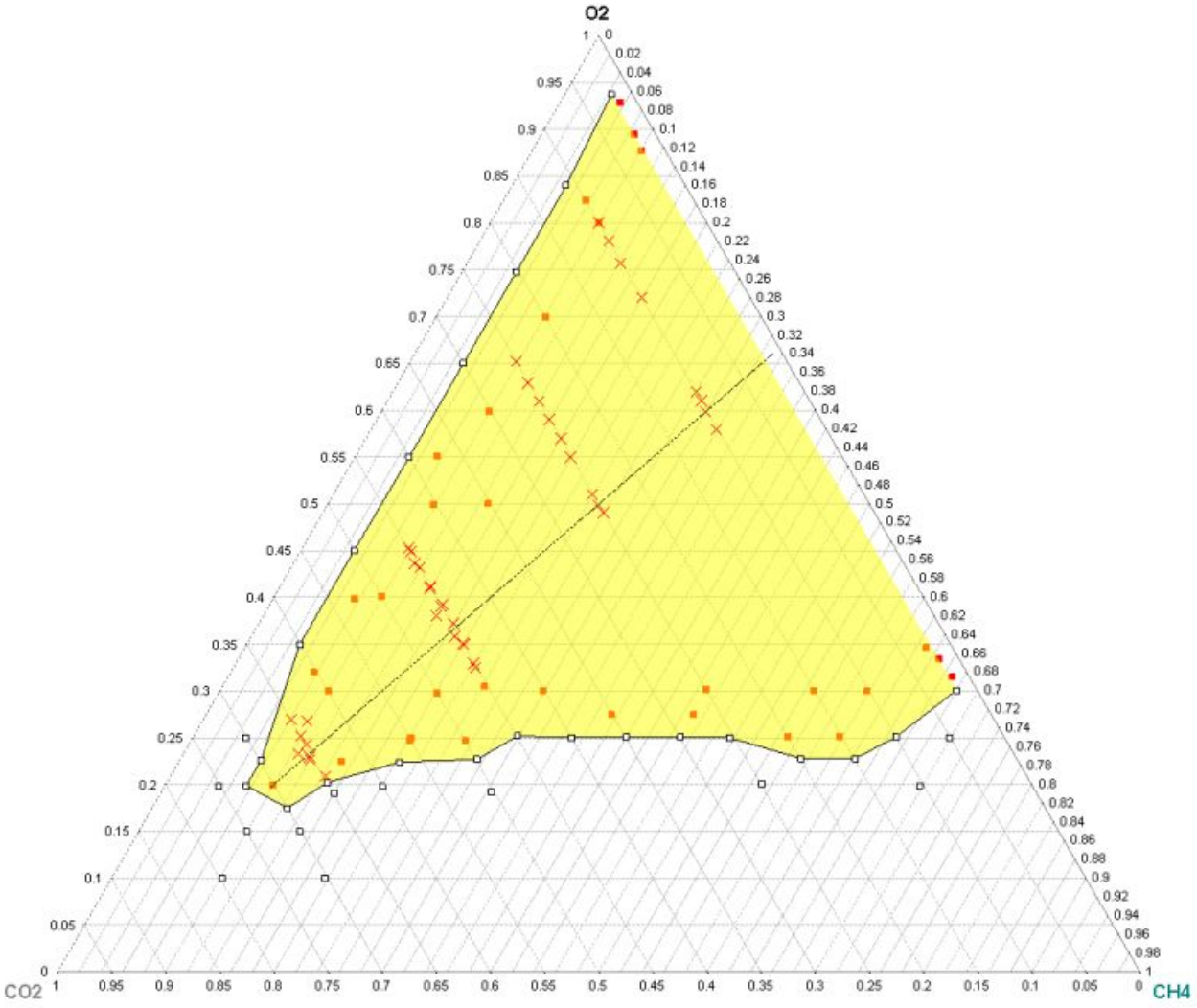

Figure S1. Safe (white) and explosive (yellow) area of any $CO_2/CH_4/O_2$ mixture.

S.2. Computational details

Equation [2] in the main paper describes the transport of species in the 2D axisymmetric model, based on diffusion coefficients (D_i^m), the mean molar mass (M_n), the multi-component diffusive flux correction term ($\boldsymbol{j}_{c,\,i}$) and the turbulent diffusive flux vector ($\boldsymbol{j}_{T,i}$), which are calculated via:

$$D_i^m = \frac{1-\omega_i}{\sum_{k\neq i}\frac{x_k}{D_{i,k}}}\,,\; M_n = \left(\sum_i \frac{\omega_i}{M_i}\right)^{-1}\,,\; \boldsymbol{j}_{c,\,i} = \rho\omega_i \sum_k \frac{M_i}{M_n} D_k^m \nabla x_k \qquad \text{[SI.4]}$$

$$\boldsymbol{j}_{T,i} = \rho\omega_i D_{T,i}\nabla\omega_i\,,\; D_{T,i} = \frac{\nu_T}{Sc_T} \qquad \text{[SI.5]}$$

Here, x_k is the mole fraction of species i, $D_{i,k}$ is the multicomponent Maxwell-Stefan diffusivity, M_i is the molar mass of species i, $D_{T,i}$ is the turbulent diffusivity coefficient of species i, ν_T is the turbulent kinematic viscosity and Sc_T is the turbulent Schmidt number.

Further, the model also solves the Reynolds-averaged Navier-Stokes equations with Menter's SST model describing turbulent flow, and μ_T in equation [4-6] in the main paper is calculated using the characteristic magnitude of the mean velocity gradients, S, using:

$$\mu_T = \rho\frac{a_1 k}{max(a_1\omega, Sf_{v2})}\,,\; S = \sqrt{2\boldsymbol{S}:\boldsymbol{S}}\,,\; \boldsymbol{S} = \frac{1}{2}\left(\nabla\boldsymbol{u} + (\nabla\boldsymbol{u})^T\right) \qquad \text{[SI.6]}$$

Here a_1 is a turbulence modelling parameter.

P in equation [5, 6] is calculated as follows:

$$P = min(P_k, 10\beta_0\rho\omega k) \qquad \text{[SI.7]}$$

$$P_k = \mu_T\left[\nabla\boldsymbol{u}:\left(\nabla\boldsymbol{u} + (\nabla\boldsymbol{u})^{\boldsymbol{T}}\right) - \frac{2}{3}(\nabla\cdot\boldsymbol{u})^2\right] - \frac{2}{3}\rho k\nabla\cdot\boldsymbol{u} \qquad \text{[SI.8]}$$

Interpolating values for parameters depending on a blending function is done as follows:

$$\varphi = f_{v1}\varphi_1 + (1-f_{v1})\varphi_2 \qquad for\ any \qquad \varphi = \gamma, \beta, \sigma_k\ or\ \sigma_\omega \qquad \text{[SI.9]}$$

Finally f_{v1} and f_{v2} are defined by:

$$f_{v1} = \tanh(\theta_1{}^4) \qquad \text{[SI.10]}$$

$$\theta_1 = min\left[max\left[\frac{\sqrt{k}}{\beta_0^*\omega l_w}, \frac{500\mu}{\rho\omega l_w}\right], \frac{4\rho\sigma_{\omega 2}k}{CD_{k\omega}l_w{}^2}\right] \qquad \text{[SI.11]}$$

$$CD_{k\omega} = max\left(\frac{2\rho\sigma_{\omega 2}}{\omega}\nabla\omega\cdot\nabla k, 10^{-10}\right) \qquad \text{[SI.12]}$$

$$f_{v2} = \tanh(\theta_2{}^2) \qquad \text{[SI.13]}$$

$$\theta_2 = max\left(\frac{2\sqrt{k}}{\beta_0^*\omega l_w}, \frac{500\mu}{\rho\omega l_w}\right) \qquad \text{[SI.14]}$$

Here l_w is the distance of the current position to the closest wall.

Table S3 - Turbulence model parameters, used in the RANS SST equations.

Parameter	Value	Parameter	Value
$\boldsymbol{a_1}$	0.31	β_0^*	0.09
$\boldsymbol{\beta_1}$	0.075	β_2	0.0828
$\boldsymbol{\gamma_1}$	0.556	γ_2	0.44
$\boldsymbol{\sigma_{k1}}$	0.85	σ_{k2}	1.0
$\boldsymbol{\sigma_{\omega 1}}$	0.5	$\sigma_{\omega 2}$	0.856

As C_p, k and k_T depend on the gas composition, which is self-consistently calculated in the model they are dependent on the mass/molar fraction of the components:

$$C_p = \sum_i \omega_i \times \frac{C_{p,i}}{M_i} \quad \text{[SI.15]}$$

Where ω_i is the weight fraction of species i, M_i is the molar mass of species i and $C_{p,i}$ refers to the heat capacity taken from the NASA polynomial of species i.[5]

$$k = 0.5\left(\sum_i x_i k_i + \frac{1}{\sum_i {x_i}/{k_i}}\right) \quad \text{[SI.16]}$$

where x_i is the molar fraction of species i, and k_i is the thermal conductivity of species i, calculated using:

$$k_i = 2.669 \times 10^{-6} \frac{\sqrt{TM_i \times 10^3}}{\sigma_i^2 \Omega_k} \times \frac{1.15C_{p,i} + 0.88R_g}{M_i} \quad \text{[SI.17]}$$

Here, σ_i is the characteristic length of the Lennard-Jones potential, and Ω_k is the dimensionless collision integral given by:

$$\Omega_k = \frac{b_1}{(T^*)^{b_2}} + \frac{b_3}{exp(b_4 T^*)} + \frac{b_5}{exp(b_6 T^*)} + \frac{4.998 \cdot 10^{-40} \mu_{D,i}^4}{k_b^2 T^* \sigma_i^6}, \quad T^* = T\frac{\varepsilon_i}{k_b} \quad \text{[SI.18]}$$

In this equation, b_x are empirical constants, $\mu_{D,i}$ is the dipole constant of species i, ε_i is the potential energy minimum value and k_b is Boltzmann's constant. These values are tabulated data taken from literature.[6]

Since we are describing a turbulent model, k_T is calculated as follows:

$$k_T = \frac{\mu_T C_p}{Pr_T} \quad \text{[SI.19]}$$

With Pr_T respresenting the turbulent Prandtl number.

Furthermore, μ and ρ also depend on the chemical composition, where the former is calculated using:

$$\mu = \sum_{i=1}^{n} \frac{\mu_i}{1 + \frac{1}{x_i}\sum_{j=1,j\neq i}^{n} x_j \phi_{ij}}, \quad \phi_{ij} = \frac{\left(1 + \left(\mu_i/\mu_j\right)^{0.5}\left(M_j/M_i\right)^{0.25}\right)^2}{\left(4/\sqrt{2}\right)\left(1 + M_i/M_j\right)^{0.5}} \qquad \text{[SI.20]}$$

In this formula, x_i is the molar fraction. The dynamic viscosity of species i, μ_i, is calculated similar to k_i in equation [SI.17], using:

$$\mu_i = 2.669 \times 10^{-6} \frac{\sqrt{TM_i \times 10^3}}{\sigma_i^2 \Omega_D} \qquad \text{[SI.21]}$$

Here, Ω_D is expressed similar to equation [SI.18]:

$$\Omega_D = \frac{b_1}{(T^*)^{b_2}} + \frac{b_3}{exp(b_4 T^*)} + \frac{b_5}{exp(b_6 T^*)} + \frac{4.998 \times 10^{-40} \mu_{D,i}^4}{k_b^2 T^* \sigma_i^6}, \quad T^* = T\frac{k_b}{\varepsilon_i} \qquad \text{[SI.22]}$$

ρ is calculated using the ideal gas law:

$$\rho = \frac{pM_N}{R_g T} \qquad \text{[SI.23]}$$

Here, p is the pressure, R_g is the gas constant, T is the temperature and M_N is the mean molar mass of the mixture.

All equations can be found in the COMSOL User Guide.[7–10]

Boundary conditions for each set of equations can be found in the tables below, directly taken from Maerivoet et al.[4]

The boundary conditions for the SST RANS equations (i.e., equations [36] in the main paper) are listed in Table S4. $\boldsymbol{u}_0$ is the inlet velocity field, $\boldsymbol{u}|_{l_w=0}$ is the velocity at the wall, $\hat{p}_0$ is the outlet pressure, I_T is the turbulent intensity, U_{ref} is the reference velocity magnitude, L_T is the turbulent length scale, β_0^* is 0.09, a turbulence model parameter, ω_{visc}^2 and ω_{log}^2 are the specific dissipation values for the linear sublayer and logarithmic layers, respectively, $\boldsymbol{n}$ is the normal vector to the boundary plane, $h_\perp$ is the reference length and l_w is the closest wall distance,

Table S4: Boundary conditions for the SST RANS (flow) equations (eq. [3-6] in the main paper).

Geometry

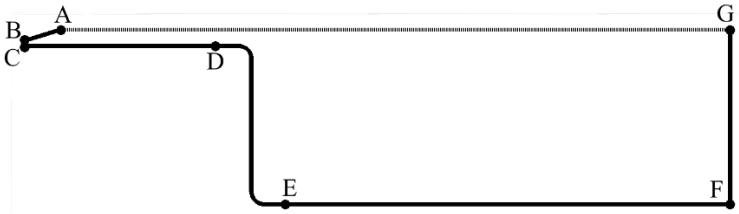

	p (Pa)	**u (m s^{-1})**	**k (m^{-2} s^{-2})**	**ω (s^{-1})**
Inlet |BC|	/	$\boldsymbol{u} = \boldsymbol{u}_0$	$k = \frac{3}{2}(U_{ref} I_T)^2$ $U_{ref} = \|\boldsymbol{u}_0\|$	$\omega = \frac{k^{0.5}}{(\beta_0^*)^{0.25} L_T}$
Walls |AB|&|CF|	/	$\boldsymbol{u}\|_{l_w=0} = \boldsymbol{0}$ $l_w = \frac{h_\perp}{2}$	$\nabla k \cdot \boldsymbol{n} = 0$	$\omega = \sqrt{\omega_{visc}^2 + \omega_{log}^2}$

Outlet |FG|	$[-p\boldsymbol{I}+\boldsymbol{K}]\boldsymbol{n}=$	/	$\nabla k \cdot \boldsymbol{n} = 0$	$\nabla \omega \cdot \boldsymbol{n} = 0$

The boundary conditions for the heat balance equation (equation 7) are listed in Table S5 Here T_{ustr} is upstream temperature, ΔH is the sensible enthalpy, $\boldsymbol{q}$ is the heat flux, q_0 is the inward heat flux, T_{ext} is the external temperature and Q_0 is the user defined heat source.

Table S5: Boundary conditions for the heat balance equation (eq. [7] in the main paper). The geometry describing the mentioned boundaries is depicted in Table S4.

	T (K)	q (W m^{-2})	Q (W m^{-3})
Inlet |BC|	$T_{ustr} = 293.15$	$-\boldsymbol{n}\cdot\boldsymbol{q} = \rho\Delta H\boldsymbol{u}\cdot\boldsymbol{n}$ $\Delta H = \int_{T_{ustr}}^{T} C_p dT$	/
Walls |CD|&|EF|	/	$-\boldsymbol{n}\cdot\boldsymbol{q} = q_0$ $q_0 = h(T_{ext} - T)$ $T_{ext} = 293.15\ K$ $h = 5\ W/m^2K$	/
Walls |AB|&|DE|	/	$-\boldsymbol{n}\cdot\boldsymbol{q} = q_0$ $q_0 = h(T_{ext} - T)$ $T_{ext} = 293.15\ K$ $h = 25\ W/m^2K$	/
Outlet |FG|	/	$-\boldsymbol{n}\cdot\boldsymbol{q} = 0$	/
Domain	/	/	$Q = Q_0$

The boundary conditions for the transport of species equation (equation [2] in the main paper) are listed in Table S6. Here $\omega_{0,i}$ is the user-defined inlet mass fraction, $\boldsymbol{j}_i$ is the diffusive flux vector of species i and D_i^m is the mixture-averaged diffusion coefficient.

Table S6: Boundary conditions for the transport of species equation (eq. [2] in the main paper). The geometry describing the mentioned boundaries is depicted in Table S4.

	ω_i (-)	J_i (mol m^{-2} s^{-1})
Inlet |BC|	$\omega_i = \omega_{0,i}$	/
Walls |AB|&|CF|	/	$-\boldsymbol{n}\cdot\boldsymbol{j}_i = \boldsymbol{0}$
Outlet |FG|	$-\boldsymbol{n}\cdot\rho D_i^m\nabla\omega_i = 0$	/

S.3. List of all chemical reactions included in the model

Table S7: List of reactions included in the model, with the rate coefficients (third column) expressed in $cm^3\ s^{-1}$ for two-body reactions, and in $cm^6\ s^{-1}$ for three-body reactions. In the rate coefficient equations, N_A is Avogadro's constant, k_B is the Boltzmann constant, R is the ideal gas constant, T_g is the gas temperature in K and n_M is the total number density of neutral species in cm^{-3}. Each reaction is written as an equilibrium reaction, and both the forward and reverse rate coefficients are listed (with the forward rate coefficients in gray background, for clarity). The references where the rate coefficients were adopted from are given in the last column. This set is reduced from an extensive chemical kinetics model, specifically for our use case of a 2D axisymmetric APGD model. Other conditions might give rise to differences in important reactions, so the reduction method has to be applied for new conditions, as described in the paper of Maerivoet et al.[4] The full chemistry set applicable for $CO_2/CH_4/O_2$ modelling is described in the paper of Slaets et al.[11]

#	Reaction	Forward rate coefficient Reverse rate coefficient	Ref. Ref.
1	$CH_4 + H \rightleftharpoons CH_3 + H_2$	$6.40 \times 10^{-24} \cdot T^{2.11} \cdot N_A \cdot \exp\left(\frac{-3900}{T}\right)$	12
		$6.62 \times 10^{-20} \cdot T^{2.24} \cdot N_A \cdot \exp\left(\frac{-3220}{T}\right)$	12
2	$CH_3 + H \rightleftharpoons CH_4$	See rate equation in footnote [a], with: $k_0 = 1.7 \times 10^{-26} \cdot T_g^{-1.8}$ $k_\infty = 3.5 \times 10^{-10}$ $F_c = 0.63 \cdot exp\left(\frac{T_g}{3.3150 \times 10^3}\right) + 0.37 \cdot exp\left(\frac{-T_g}{6.10 \times 10^1}\right)$	13
		See rate equation in footnote [a], with: $k_0 = 7.5 \times 10^{-7} \cdot exp\left(\frac{-4.570 \times 10^4}{T_g}\right)$ $k_\infty = 2.4 \times 10^{16} \cdot exp\left(\frac{-5.280 \times 10^4}{T_g}\right)$ $F_c = exp\left(\frac{-T_g}{1.350 \times 10^3}\right) + exp\left(\frac{-7.8340 \times 10^3}{T_g}\right)$	13
3	$CH_3 + CH_4 \rightleftharpoons C_2H_6 + H$	$8 \times 10^7 \cdot exp\left(\frac{-1.6736 \times 10^5}{R \cdot T_g}\right)$	14
		$k_{rev} \cdot K_{eq}$	b
4	$CH_3 + CH_4 \rightleftharpoons C_2H_5 + H_2$	$1 \times 10^7 \cdot exp\left(\frac{-9.6232 \times 10^4}{R \cdot T_g}\right)$	14
		$k_{rev} \cdot K_{eq}$	b

5	$CH_3 + CH_3 \rightleftharpoons C_2H_6$	See rate equation in footnote [a], with: $k_0 = 3.5 \times 10^{-7} \cdot T_g^{-7} \cdot exp\left(\frac{-1.39 \times 10^3}{T_g}\right)$ $k_\infty = 6 \times 10^{-11}$ $F_c = 0.38 \cdot exp\left(\frac{-T_g}{7.3 \times 10^1}\right) + 0.62 exp\left(\frac{-T_g}{1.18 \times 10^3}\right)$	13
		See rate equation in footnote [a], with: $k_0 = 2.6 \times 10^{25} \cdot T_g^{-8.73} \cdot exp\left(\frac{-4.729 \times 10^4}{T_g}\right)$ $k_\infty = 4.5 \times 10^{21} \cdot T_g^{-1.37} \cdot exp\left(\frac{-4.59 \times 10^4}{T_g}\right)$ $F_c = 0.38 \cdot exp\left(\frac{-T_g}{7.3 \times 10^1}\right) + 0.62 \cdot exp\left(\frac{-T_g}{1.18 \times 10^3}\right)$	13
6	$CH_3 + CH_3 \rightleftharpoons C_2H_5 + H$	$9 \times 10^{-17} \cdot N_A \cdot exp\left(\frac{-8.08 \times 10^3}{T_g}\right)$	13
		7×10^{-17}	13
7	$C_2H_5 + H_2 \rightleftharpoons C_2H_6 + H$	$5.1 \times 10^{-30} \cdot N_A \cdot T_g^{3.6} \cdot exp\left(\frac{-4.253 \times 10^3}{T_g}\right)$	13
		$1.63 \times 10^{-16} \cdot N_A \cdot exp\left(\frac{-4.640 \times 10^3}{T_g}\right)$	13
8	$C_2H_2 + H \rightleftharpoons C_2H + H_2$	$3.0 \times 10^{-19} \cdot N_A \cdot exp\left(\frac{-8.700 \times 10^3}{T_g}\right)$	13
		$3.6 \times 10^{-20} \cdot N_A \cdot T_g^{0.94} \cdot exp\left(\frac{-3.28 \times 10^2}{T_g}\right)$	13
9	$C_2H_6 + CH_3 \rightleftharpoons C_2H_5 + CH_4$	$9.3 \times 10^{-20} \cdot N_A \cdot exp\left(\frac{-4.740 \times 10^3}{T_g}\right)$ $+1.4 \times 10^{-15} \cdot N_A \cdot exp\left(\frac{-1.120 \times 10^4}{T_g}\right)$	15
		$1.43 \times 10^{-31} \cdot N_A \cdot T_g^{4.14} \cdot exp\left(\frac{-6.322 \times 10^3}{T_g}\right)$	15
10	$C_2H_2 + CH_3 \rightleftharpoons C_2H + CH_4$	$3 \times 10^{-19} \cdot N_A \cdot exp\left(\frac{-8.7 \times 10^3}{T_g}\right)$	15
		$3.6 \times 10^{-20} \cdot T_g^{0.94} \cdot N_A \cdot exp\left(\frac{-3.28 \times 10^2}{T_g}\right)$	13
11	$C_2H_6 \rightleftharpoons C_2H_5 + H$	See rate equation in footnote [a], with: $k_0 = \frac{10^{42.839}}{n_M} \cdot T_g^{-6.431} \cdot exp\left(\frac{-5.3938 \times 10^4}{T_g}\right)$	16

		$k_\infty = 10^{20.947} \cdot T_g^{-1.228} \cdot exp\left(\frac{-5.1439 \times 10^4}{T_g}\right)$ $F_c = 47.61 \cdot exp\left(\frac{-1.6182 \times 10^4}{T_g}\right) + exp\left(\frac{-T_g}{3.371 \times 10^3}\right)$	
		$\frac{6 \times 10^{-17} \cdot N_A}{1 + 10^{-1.915+2.69\times10^3 \cdot T_g - 2.35\times10^{-7} \cdot T_g^2}}$	15
12	$C_2H_5 \rightleftharpoons C_2H_4 + H$	See rate equation in footnote [a], with: $k_0 = 1.7 \times 10^{-6} \cdot exp\left(\frac{-1.68 \times 10^4}{T_g}\right)$ $k_\infty = 8.2 \times 10^{13} \cdot exp\left(\frac{-2.007 \times 10^4}{T_g}\right)$ $F_c = 0.25 \cdot exp\left(\frac{-T_g}{9.7 \times 10^1}\right) + 0.75 \cdot exp\left(\frac{-T_g}{1.379 \times 10^3}\right)$	13
		See rate equation in footnote [a], with: $k_0 = 1.3 \times 10^{-29} \cdot exp\left(\frac{-3.8 \times 10^2}{T_g}\right)$ $k_\infty = 6.6 \times 10^{-15} \cdot T_g^{1.28} \cdot exp\left(\frac{-6.5 \times 10^2}{T_g}\right)$ $F_c = 0.24 \cdot exp\left(\frac{-T_g}{4 \times 10^1}\right) + 0.76 \cdot exp\left(\frac{-T_g}{1.025 \times 10^3}\right)$	13
13	$C_2H_4 \rightleftharpoons C_2H_2 + H_2$	$10^{12.9} \cdot T_g^{0.44} \cdot exp\left(\frac{-4.467 \times 10^4}{T_g}\right)$	15
		$5 \times 10^{-19} \cdot N_A \cdot exp\left(\frac{-1.96 \times 10^4}{T_g}\right)$	15
14	$C_2H + H \rightleftharpoons C_2H_2$	$3 \times 10^{-16} \cdot N_A$	15
		$10^{15.42} \cdot exp\left(\frac{-6.2445 \times 10^4}{T_g}\right)$	15
15	$M + CO_2 \rightleftharpoons M + CO + O$	$3.65 \times 10^8 \cdot exp\left(\frac{-5.2525 \times 10^4}{T_g}\right)$	17
		$2.79 \times 10^{-41} \cdot T_g^{-1.5} \cdot N_A \cdot exp\left(\frac{-2.520 \times 10^3}{T_g}\right)$	15
16	$H + OH \rightleftharpoons H_2 + O$	$4.1 \times 10^{-18} \cdot \frac{T_g}{3 \times 10^2} \cdot N_A \cdot exp\left(\frac{-3.50 \times 10^3}{T_g}\right)$	18
		$9 \times 10^{-18} \cdot \left(\frac{T_g}{3 \times 10^2}\right)^{1.0} \cdot N_A \cdot exp\left(\frac{-4.480 \times 10^3}{T_g}\right)$	18

17	$M + H_2O \rightleftharpoons M + H + OH$	$5.9 \times 10^{-13} \cdot \left(\frac{T_g}{3 \times 10^2}\right)^{-2.2} \cdot N_A \cdot exp\left(\frac{-5.90 \times 10^4}{T_g}\right)$	18
		$k_{rev} \cdot K_{eq}$	b
18	$OH + OH \rightleftharpoons H_2O + O$	$1.02 \times 10^{-18} \cdot \left(\frac{T_g}{3 \times 10^2}\right)^{1.4} \cdot N_A \cdot exp\left(\frac{2.0 \times 10^2}{T_g}\right)$	15
		$7.6 \times 10^{-21} \cdot T_g^{1.3} \cdot N_A \cdot exp\left(\frac{-8.6 \times 10^3}{T_g}\right)$	15
19	$M + OH \rightleftharpoons M + H + O$	$4.7 \times 10^{-14} \cdot \left(\frac{T_g}{3 \times 10^2}\right)^{-1.0} \cdot N_A \cdot exp\left(\frac{5.0830 \times 10^4}{T_g}\right)$	18
		$4.33 \times 10^{-44} \cdot \left(\frac{T_g}{3 \times 10^2}\right)^{-1} \cdot {N_A}^2$	15
20	$H_2 + OH \rightleftharpoons H + H_2O$	$3.6 \times 10^{-22} \cdot T_g^{1.52} \cdot N_A \cdot exp\left(\frac{-1.74 \times 10^3}{T_g}\right)$	13
		$7.5 \times 10^{-22} \cdot T_g^{1.6} \cdot N_A \cdot exp\left(\frac{-9.03 \times 10^3}{T_g}\right)$	13
21	$HO_2 + OH \rightleftharpoons H_2O + O_2$	$8.05 \times 10^{-17} \cdot N_A \cdot \left(\frac{T_g}{3 \times 10^2}\right)^{-1.0}$	15
		$4.3 \times 10^{-18} \cdot \left(\frac{T_g}{3 \times 10^2}\right)^{0.5} \cdot N_A \cdot exp\left(\frac{-3.660 \times 10^4}{T_g}\right)$	18
22	$H + HO_2 \rightleftharpoons H_2 + O_2$	$1.1 \times 10^{-16} \cdot N_A \cdot exp\left(\frac{-1.070 \times 10^3}{T_g}\right)$	15
		$3.2 \times 10^{-17} \cdot N_A \cdot exp\left(\frac{-2.410 \times 10^4}{T_g}\right)$	18
23	$H + HO_2 \rightleftharpoons OH + OH$	$2.8 \times 10^{-16} \cdot N_A \cdot exp\left(\frac{-4.40 \times 10^2}{T_g}\right)$	15
		$2 \times 10^{-17} \cdot N_A \cdot exp\left(\frac{-2.020 \times 10^4}{T_g}\right)$	18
24	$O + OH \rightleftharpoons H + O_2$	$4.33 \times 10^{-17} \cdot \left(\frac{T_g}{3 \times 10^2}\right)^{-0.5} \cdot N_A \cdot exp\left(\frac{-3.0 \times 10^1}{T_g}\right)$	15
		$1.62 \times 10^{-16} \cdot N_A \cdot exp\left(\frac{-7.4740 \times 10^3}{T_g}\right)$	19
25	$M + H + O_2 \rightleftharpoons M + HO_2$	$3.33 \times 10^{-43} \cdot \left(\frac{T_g}{3 \times 10^2}\right)^{-1} \cdot {N_A}^2$	13
		$k_{rev} \cdot K_{eq}$	b
26	$CO_2 + H \rightleftharpoons CO + OH$	$4.7 \times 10^{-16} \cdot N_A \cdot exp\left(\frac{-1.3915 \times 10^4}{T_g}\right)$	13

		$3.3 \times 10^{0} \cdot T_g^{1.55} \cdot exp\left(\frac{4.02 \times 10^{2}}{T_g}\right)$	20
27	M + CO + H ⇌ M + HCO	$2 \times 10^{-47} \cdot T_g^{0.2} \cdot {N_A}^2$	13
		$k_{rev} \cdot K_{eq}$	b
28	CH_4 + O ⇌ CH_3 + OH	$7.3 \times 10^{-25} \cdot T_g^{2.5} \cdot N_A \cdot exp\left(\frac{-3.31 \times 10^{3}}{T_g}\right)$	13
		$1.16 \times 10^{-25} \cdot T_g^{2.2} \cdot N_A \cdot exp\left(\frac{-2.24 \times 10^{3}}{T_g}\right)$	21
29	CH_4 + O_2 ⇌ CH_3 + HO_2	$8.1 \times 10^{-25} \cdot T_g^{2.5} \cdot N_A \cdot exp\left(\frac{-2.637 \times 10^{4}}{T_g}\right)$	13
		$6 \times 10^{-18} \cdot N_A$	15
30	CH_3 + O ⇌ H + HCHO	$1.12 \times 10^{-16} \cdot N_A$	13
		$k_{rev} \cdot K_{eq}$	b
31	CH_3 + O ⇌ CO + H_2 + H	$0.28 \times 10^{-16} \cdot N_A$	13
		$k_{rev} \cdot K_{eq}$	b
32	CH_3 + O_2 ⇌ HCHO + OH	$3.7 \times 10^{-18} \cdot N_A \cdot exp\left(\frac{-1.114 \times 10^{4}}{T_g}\right)$	13
		$k_{rev} \cdot K_{eq}$	b
33	CH_3 + O_2 ⇌ CH_3O + O	$3.5 \times 10^{-18} \cdot N_A \cdot exp\left(\frac{-1.634 \times 10^{4}}{T_g}\right)$	13
		$1.875 \times 10^{-17} \cdot N_A$	13
34	CH_4 + OH ⇌ CH_3 + H_2O	$1.66 \times 10^{-24} \cdot T_g^{2.182} \cdot N_A \cdot exp\left(\frac{-1.231 \times 10^{3}}{T_g}\right)$	22
		$8 \times 10^{-28} \cdot T_g^{2.9} \cdot N_A \cdot exp\left(\frac{-7.48 \times 10^{3}}{T_g}\right)$	23
35	CH_3 + HO_2 ⇌ CH_3O + OH	$3 \times 10^{-17} \cdot N_A$	13
		$k_{rev} \cdot K_{eq}$	b
36	H + HCO ⇌ CO + H_2	$1.5 \times 10^{-16} \cdot N_A$	13
		$k_{rev} \cdot K_{eq}$	b
37	HCHO + OH ⇌ H_2O + HCO	$2.31 \times 10^{-17} \cdot N_A \cdot exp\left(\frac{-3.04 \times 10^{2}}{T_g}\right)$	13
		$3.9 \times 10^{-22} \cdot T_g^{1.35} \cdot N_A \cdot exp\left(\frac{-1.3146 \times 10^{4}}{T_g}\right)$	15

38	$HCO + O_2 \rightleftharpoons CO + HO_2$	$4.5 \times 10^{-20} \cdot T_g^{0.68} \cdot N_A \cdot exp\left(\frac{2.36 \times 10^2}{T_g}\right)$	13
		$k_{rev} \cdot K_{eq}$	b
39	$CH_3 + HCO \rightleftharpoons CH_4 + CO$	$2 \times 10^{-16} \cdot N_A$	15
		$k_{rev} \cdot K_{eq}$	b
40	$CH_3 + HCHO \rightleftharpoons CH_4 + HCO$	$5.3 \times 10^{-29} \cdot T_g^{3.36} \cdot N_A \cdot exp\left(\frac{-2.17 \times 10^3}{T_g}\right)$	13
		$1.21 \times 10^{-26} \cdot T_g^{2.85} \cdot N_A \cdot exp\left(\frac{-1.133 \times 10^4}{T_g}\right)$	15
41	$C_2H_4 + OH \rightleftharpoons CH_3 + HCHO$	$\frac{1}{3} \cdot 3.4 \times 10^{-17} \cdot N_A \cdot exp\left(\frac{-2.99 \times 10^3}{T_g}\right)$	13
		$k_{rev} \cdot K_{eq}$	b
42	$C_2H_2 + OH \rightleftharpoons CH_2CO + H$	$0.5 \cdot 1.3 \times 10^{-16} \cdot N_A \cdot exp\left(\frac{-6.8 \times 10^3}{T_g}\right)$	13
		$k_{rev} \cdot K_{eq}$	b
43	$C_2H_4 + O \rightleftharpoons CH_3 + HCO$	$0.6 \cdot 2.25 \times 10^{-23} \cdot T_g^{1.88} \cdot N_A \cdot exp\left(\frac{-9.2 \times 10^1}{T_g}\right)$	13
		$k_{rev} \cdot K_{eq}$	b
44	$C_2H_4 + O \rightleftharpoons CH_2CO + H_2$	$0.05 \cdot 2.25 \times 10^{-23} \cdot T_g^{1.88} \cdot N_A \cdot exp\left(\frac{-9.2 \times 10^1}{T_g}\right)$	13
		$k_{rev} \cdot K_{eq}$	b
45	$C_2H_2 + O \rightleftharpoons H + HCCO$	$0.8 \cdot 1.95 \times 10^{-21} \cdot T_g^{1.4} \cdot N_A \cdot exp\left(\frac{-1.11 \times 10^3}{T_g}\right)$	13
		$k_{rev} \cdot K_{eq}$	b
46	$CH_2CO + H \rightleftharpoons CH_3 + CO$	$1.11 \times 10^{-1} \cdot T_g^2 \cdot exp\left(\frac{-2 \times 10^3 \cdot 4.184}{R \cdot T_g}\right)$	24
		$k_{rev} \cdot K_{eq}$	b
47	$HCCO + O \rightleftharpoons CO + CO + H$	$1.6 \times 10^{-16} \cdot N_A - 4.9 \times 10^{-17} \cdot N_A \cdot exp\left(\frac{-5.6 \times 10^2}{T_g}\right)$	13
		$k_{rev} \cdot K_{eq}$	b
48	$CH_2CO + CH_3 \rightleftharpoons C_2H_5 + CO$	$1.24 \times 10^{-1} \cdot T_g^{2.29} \cdot exp\left(\frac{-1.0642 \times 10^4 \cdot 4.184}{R \cdot T_g}\right)$	17
		$k_{rev} \cdot K_{eq}$	b
49	$M + HCHO \rightleftharpoons M + H + HCO$	$8.09 \times 10^{-15} \cdot N_A \cdot exp\left(\frac{-3.805 \times 10^4}{T_g}\right)$	13

		$k_{rev} \cdot K_{eq}$	b
50	M + HCHO ⇌ M + CO + H_2	$4.7 \times 10^{-15} \cdot N_A \cdot exp\left(\frac{-3.211 \times 10^4}{T_g}\right)$	13
		$k_{rev} \cdot K_{eq}$	b
51	H + HCHO ⇌ CH_3O	$2.4 \times 10^7 \cdot exp\left(\frac{-4.11 \times 10^3 \cdot 4.184}{T_g}\right)$	25
		$k_{rev} \cdot K_{eq}$	b
52	CH_3O + CO ⇌ CH_3 + CO_2	$2.6 \times 10^{-17} \cdot N_A \cdot exp\left(\frac{-5.94 \times 10^3}{T_g}\right)$	15
		$k_{rev} \cdot K_{eq}$	b
53	HCO + OH ⇌ CO + H_2O	$1.8 \times 10^{-16} \cdot N_A$	13
		$k_{rev} \cdot K_{eq}$	b
54	HCO + HCO ⇌ CO + HCHO	$4.265 \times 10^{-17} \cdot N_A$	13
		$k_{rev} \cdot K_{eq}$	b
55	CH_2CO + H ⇌ H_2 + HCCO	$1.8 \times 10^8 \cdot exp\left(\frac{-8.6 \times 10^3 \cdot 4.184}{R \cdot T_g}\right)$	24
		$k_{rev} \cdot K_{eq}$	b
56	CH_2CO + OH ⇌ CH_3 + CO_2	$0.37 \cdot 2.8 \times 10^{-18} \cdot N_A \cdot exp\left(\frac{5.1 \times 10^2}{T_g}\right)$	13
		$k_{rev} \cdot K_{eq}$	b
57	CH_2CO + CH_3 ⇌ CH_4 + HCCO	$1.55 \times 10^{-4} \cdot T_g^{3.38} \cdot exp\left(\frac{-1.0512 \times 10^3 \cdot 4.184}{R \cdot T_g}\right)$	17
		$k_{rev} \cdot K_{eq}$	b

Constants:
$N_A = 6.02214076 \times 10^{23}\ mol^{-1}$
$k_B = 1.38064852 \times 10^{-23}\ JK^{-1}$
$R = 8.31446261815324\ JK^{-1}mol^{-1}$
n_M = total number density of neutral species (cm^{-3})

Notes: [a] falloff expression, Lindemann-Hinshelwood expression with broadening factor:

$$k = \frac{k_0[M]k_\infty}{k_0[M] + k_\infty} F; \log F = \frac{\log F_c}{1 + \left[\frac{\log(k_0[M]/k_\infty)}{N}\right]^2}; N = 0.75 - 1.27 \log F_c$$

[b] Reaction rate coefficient expression calculated from equilibrium constant and reverse reaction rate:

$$K_{eq} = e^{\left(\frac{-\Delta G_r}{RT}\right)} \cdot \left(\frac{p}{RT}\right)^{\Delta v}; p = 1bar; \Delta v = \sum \mu_P - \sum \mu_R$$

S.4. Carbon deposit analysis for "without O_2" sample

In section 3.2 of the main text, the analyses of the solid carbon deposits are shown for an experiment with O_2 added. Here, in Figure S2, the same analyses are presented for a sample that was formed in a plasma without O_2 added. Similarly, heavy spherical particles are commonly found on the carbon structures. The EDX analysis reveals a similar stainless steel composition as for the other sample. Further, the TEM analyses yield the same results as for the "with O_2" sample, being a carbon structure consisting of planar carbon, without much additional ordering. Again, this carbon material could be characterized as so-called turbostratic carbon.

Overall, no significant differences were observed between the solid carbon samples formed with and without O_2 added.

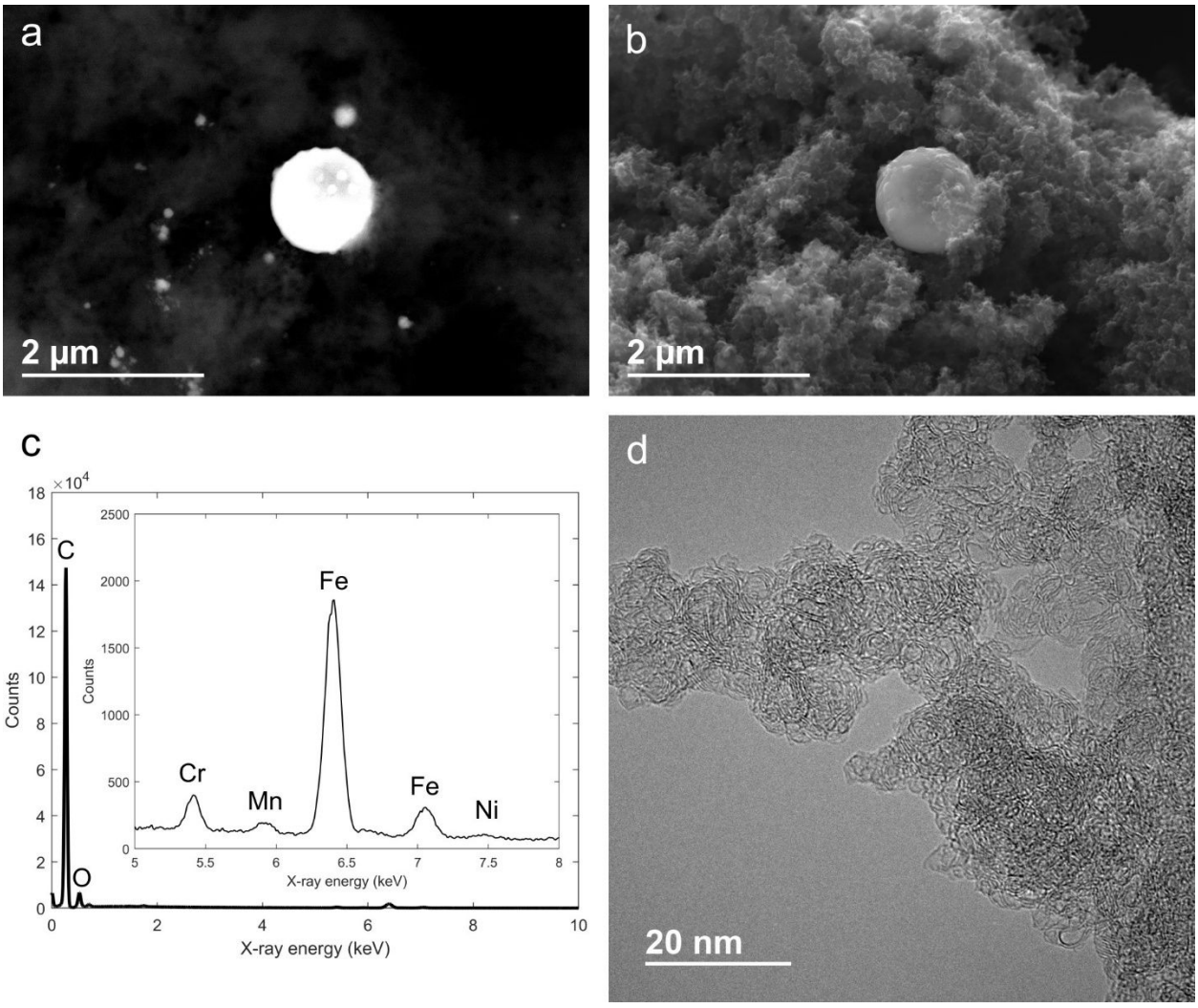

Figure S2. SEM, EDX, and TEM data for the carbon collected at the anode after an experiment without O_2 added with a 65/35/0 ratio. A: Backscattered electron SEM image, highlighting a heavy, spherical particle, with smaller heavy particles around. B: Secondary electron SEM image of the same area as in A, showing the microscopic structure of the carbon surrounding the heavy

spherical particles. The carbon material appears to consist of a large agglomerate of smaller structures. C: EDX spectrum of the heavy particle presented in A, the inset shows the same spectrum but zoomed in on a relevant energy range, proving that the heavy particle is in fact stainless steel (containing Fe, Cr, and small amounts of Ni and Mn). D: Representative BF-TEM image of the carbon material. The material consists of layers of graphene-like carbon that are not structured, indicating the material is not crystalline, but also not fully amorphous.

S.5. The energy cost of syngas

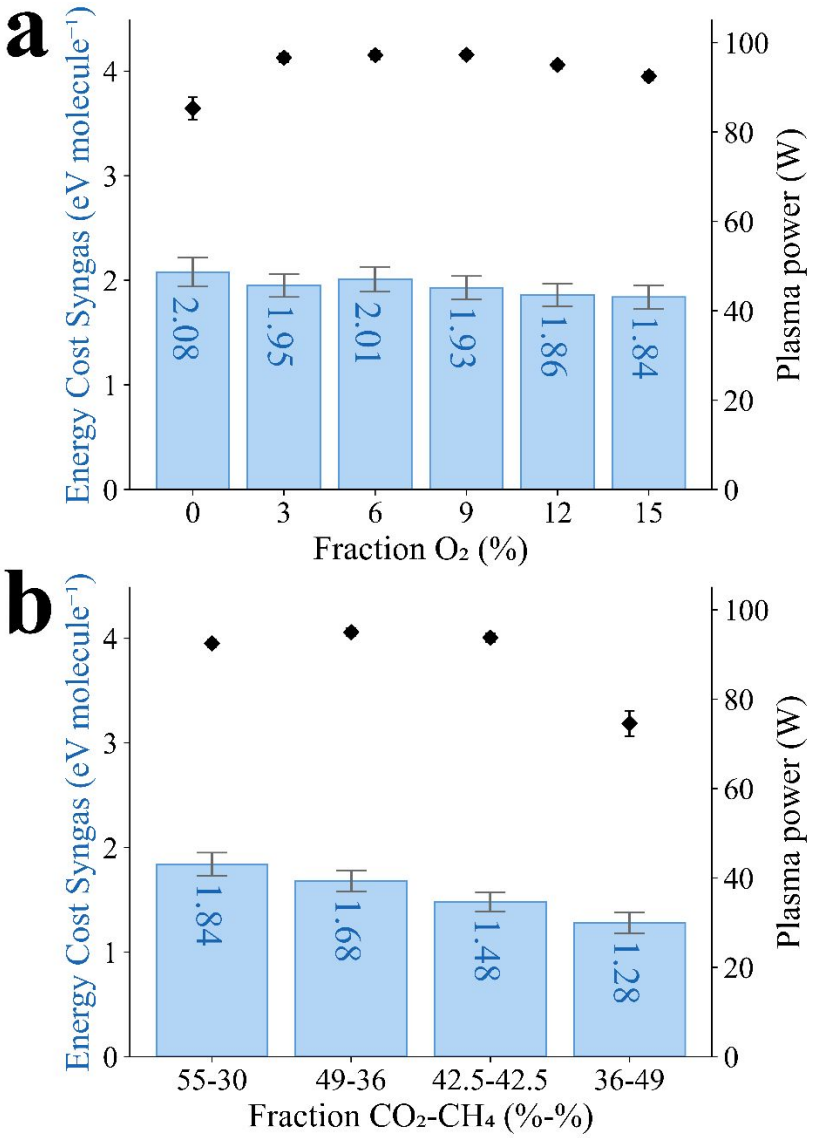

Figure S3. Energy cost of syngas in eV molecule^{-1}, as well as plasma power (right y-axis), as a function of O_2 fraction (a, series A), and CO_2/CH_4 fraction (b, series B). Error bars are based on three successive experiments.

Bibliography

(1) Pinhão, N.; Moura, A.; Branco, J.; Neves, J. Influence of Gas Expansion on Process Parameters in Non-Thermal Plasma Plug-Flow Reactors: A Study Applied to Dry Reforming of Methane. *Int. J. Hydrog. Energy* **2016**, *41* (22), 9245–9255.

(2) Cleiren, E.; Heijkers, S.; Ramakers, M.; Bogaerts, A. Dry Reforming of Methane in a Gliding Arc Plasmatron: Towards a Better Understanding of the Plasma Chemistry. *Wiley Online Libr.* **2017**, *10* (20), 4025–4036. https://doi.org/10.1002/cssc.201701274.

(3) Wanten, B.; Vertongen, R.; De Meyer, R.; Bogaerts, A. Plasma-Based CO2 Conversion: How to Correctly Analyze the Performance? *J. Energy Chem.* **2023**, *86*, 180–196. https://doi.org/10.1016/j.jechem.2023.07.005.

(4) Maerivoet, S.; Tsonev, I.; Slaets, J.; Reniers, F.; Bogaerts, A. Coupled Multi-Dimensional Modelling of Warm Plasmas: Application and Validation for an Atmospheric Pressure Glow Discharge in CO2/CH4/O2. *Chem. Eng. J.* **2024**, *492*, 152006. https://doi.org/10.1016/J.CEJ.2024.152006.

(5) McBride, B. J.; Zehe, M. J.; Gordon, S. NASA Glenn Coefficients for Calculating Thermodynamic Properties of Individual Species: National Aeronautics and Space Administration. *John H. Glenn Res. Cent. Lewis F.* **2002**, No. September, 295.

(6) Menter, F. R.; Kuntz, M.; Langtry, R. Ten Years of Industrial Experience with the SST Turbulence Model Turbulence Heat and Mass Transfer. *Heat Mass Transf.* **2003**, *4* (July 2014), 625–632.

(7) Comsol Multiphysics 6.0 Heat Transfer Module User's Guide.

(8) Comsol Multiphysics 6.0 CFD Module User's Guide.

(9) Comsol Multiphysics 6.0 Chemical Reaction Engineering Module User's Guide.

(10) COMSOL Multiphysics 6.0 (Available at: Www.Comsol.Com).

(11) Slaets, J.; Loenders, B.; Bogaerts, A. Plasma-Based Dry Reforming of CH4: Plasma Effects vs. Thermal Conversion. *Fuel* **2024**, *360*. https://doi.org/10.1016/j.fuel.2023.130650.

(12) Rabinowitz, M. J.; Sutherland, J. W.; Patterson, P. M.; Klemm, R. B. Direct Rate Constant Measurements for H + CH4 → CH3 + H2, 897-1729 K, Using the Flash Photolysis-Shock Tube Technique. *J. Phys. Chem.* **1991**, *95* (2), 674–681. https://doi.org/10.1021/j100155a033.

(13) Baulch, D. L.; Bowman, C. T.; Cobos, C. J.; Cox, R. A.; Just, T.; Kerr, J. A.; Pilling, M. J.; Stocker, D.; Troe, J.; Tsang, W.; Walker, R. W.; Warnatz, J. Evaluated Kinetic Data for Combustion Modeling: Supplement II. *J. Phys. Chem. Ref. Data* **2005**, *34* (3), 757–1397. https://doi.org/10.1063/1.1748524.

(14) Tabayashi, K.; Bauer, S. H. The Early Stages of Pyrolysis and Oxidation of Methane. *Combust. Flame* **1979**, *34* (C), 63–83. https://doi.org/10.1016/0010-2180(79)90079-8.

(15) Tsang, W.; Hampson, R. F. Chemical Kinetic Data Base for Combustion Chemistry. Part I. Methane and Related Compounds. *J. Phys. Chem. Ref. Data* **1986**, *15* (3), 1087–1279. https://doi.org/10.1063/1.555759.

(16) Stewart, P. H.; Larson, C. W.; Golden, D. M. Pressure and Temperature Dependence of Reactions Proceeding via a Bound Complex. 2. Application to 2CH3 → C2H5 + H. *Combust. Flame* **1989**, *75* (1), 25–31. https://doi.org/10.1016/0010-2180(89)90084-9.

(17) Semenikhin, A. S.; Shubina, E. G.; Savchenkova, A. S.; Chechet, I. V; Matveev, S. G.; Konnov, A. A.; Mebel, A. M. Mechanism and Rate Constants of the CH3+ CH2CO Reaction: A Theoretical Study. *Int. J. Chem. Kinet.* **2018**, *50* (4), 273–284. https://doi.org/10.1002/kin.21156.

(18) Capitelli, M.; Ferreira, C. M.; Gordiets, B. F.; Osipov, A. I. Plasma Kinetics in Atmospheric Gases. *Plasma Phys. Control. Fusion* **2001**, *43* (3), 371–372. https://doi.org/10.1088/0741-3335/43/3/702.

(19) Baulch, D. L.; Pilling, M. J.; Cobos, C. J.; Cox, R. A.; Frank, P.; Hayman, G.; Just, T.; Kerr, J. A.; Murrells, T.; Troe, J.; Walker, R. W.; Warnatz, J. Evaluated Kinetic Data for Combustion Modeling. Supplement I. *J. Phys. Chem. Ref. Data* **1994**, *23* (6), 847–848. https://doi.org/10.1063/1.555953.

(20) Lissianski, V.; Yang, H.; Qin, Z.; Mueller, M. R.; Shin, K. S.; Gardiner, W. C. High-Temperature Measurements of the Rate Coefficient of the H + CO2 → CO + OH Reaction. *Chem. Phys. Lett.* **1995**, *240* (1–3), 57–62. https://doi.org/10.1016/0009-2614(95)00496-Q.

(21) Cohen, N.; Westberg, K. R. Chemical Kinetic Data Sheets for High-Temperature Reactions. Part II. *J. Phys. Chem. Ref. Data* **1991**, *20* (6), 1211–1311. https://doi.org/10.1063/1.555901.

(22) Srinivasan, N. K.; Su, M. C.; Sutherland, J. W.; Michael, J. V. Reflected Shock Tube Studies of High-Temperature Rate Constants for OH + CH 4 → CH 3 + H 2O and CH 3 + NO 2 → CH 3O + NO. *J. Phys. Chem. A* **2005**, *109* (9), 1857–1863. https://doi.org/10.1021/jp040679j.

(23) Cohen, N.; Westberg, K. R. Chemical Kinetic Data Sheets for High Temperature Chemical Reactions. *J. Phys. Chem. Ref. Data* **1983**, *12* (3), 531–590. https://doi.org/10.1063/1.555692.

(24) Hidaka, Y.; Sato, K.; Yamane, M. High-Temperature Pyrolysis of Dimethyl Ether in Shock Waves. *Combust. Flame* **2000**, *123* (1–2), 1–22. https://doi.org/10.1016/S0010-2180(00)00122-X.

(25) Curran, H. J. Rate Constant Estimation for C1 to C4 Alkyl and Alkoxyl Radical Decomposition. *Int. J. Chem. Kinet.* **2006**, *38* (4), 250–275. https://doi.org/10.1002/kin.20153.